PCCP

Accepted Manuscript

ROYAL SOCIETY OF CHEMISTRY

www.rsc.org/pccp

Physical Chemistry Chemical Physics
CREATED USING THE RSC LaTeX PCCP ARTICLE TEMPLATE – SEE www.rsc.org/electronicfiles FOR DETAILS
ARTICLE TYPE www. rsc.org/xxxxxx | XXXXXXXX

OH-stretch overtone of methanol: empirical assignment using two temperature technique in supersonic jet†

Vít Svoboda,[a,b] Veronika Horká-Zelenková,[a] Jozef Rakovský,[a] Petr Pracna, [a] and Ondrej Votava [a,*]

Received Xth XXXXXXXXXX 20XX, Accepted Xth XXXXXXXXX 20XX
First published on the web Xth XXXXXXXXXX 200X
DOI: 10.1039/b000000x

This paper describes a novel approach for empirical lower state assignments in complex high resolution ro-vibrational overtone spectra of molecules with low rotational constants and complex intramolecular dynamics. Methanol, CH_3OH, was chosen as a representative of such molecules – it is an asymmetric top with two non-hydrogen nuclei and hindered internal rotation leading to dense and disordered rotational structure of vibrational overtone bands. We report the first rotationally resolved methanol spectra of the OH-stretch overtone $2\nu_1$ band using sub-Doppler diode laser spectroscopy in supersonic jet, and describe how combination of two temperature analysis (TTA) and analysis by ground state combination differences (GSCDs) is used to reliably identify spectral lines that originate from lowest rotational states. In the first step of the analysis, the TTA was utilized to obtain a set of possible rotational assignments for each spectral line using the line intensity variation between two different temperatures in the supersonic jet (13, and 56 K respectively). Thereafter, the GSCDs were used to confirm specific lower state assignment for those spectral lines that have been identified to have low rotational ground states by the TTA. We show that the TTA pre-selection leads to fast and reliable confirmation by GSCDs and avoids false assignments due to accidental GSCD matches. The procedure yields an important subset of reliably assigned spectral lines in the complex ro-vibrational structure that provides a convenient starting point for subsequent application of traditional spectral analysis techniques.

1 Introduction

High resolution overtone spectra are in general complicated and often show many irregularities in their ro-vibrational structure. This is caused by high density of vibrational states and strong anharmonic and rotation-vibration couplings. Resulting complex spectra are often hard to assign using standard spectroscopic approaches developed for the fundamental ro-vibrational bands. To unravel such spectra additional experimental information is needed to guide the theoretical interpretation. Two temperature technique in the supersonic jet is a promising strategy to determine the lower state energies from the ratio of the line intensities measured at different temperatures and thus provide additional information on the measured spectra.

Assignment approaches based on spectra temperature dependence have so far been only effectively tested for small light molecules such as CH_4 and NH_3 [1–11]. Initially the technique has been used with spectra measured at room and reduced temperatures in absorption cells (cell-cell measurement). We have extended the method for CH_4 by combining measurements in liquid N_2 cooled cell and in supersonic jet expansion (cell-jet measurement) [12–14] and finally we applied the technique for measurements in supersonic molecular beam only (jet-jet technique) which has been tested on NH_3 [15]. All the previously studied molecules have large rotational constants, and thus rotational levels are widely spaced in energy. In such case the TTA gives well determined assignments of the rotational levels particularly for low J'' states.

In this paper we explore the applicability of the two temperature technique for larger molecules with more complicated structure and intramolecular dynamics. Large molecules have in general smaller rotational constants and low frequency vibrational modes are often present that couple with the overall rotation to produce complicated structure of ro-vibrational levels. Consequently rotational states are closely spaced and more states are populated at given temperature compared to smaller species. Very precise determination of the empirical lower state energies would be required to unambiguously assign the rotational quantum numbers based on the two temperature technique alone.

We have chosen methanol as a prototypical molecule for such study. It is a near-prolate top asymmetric rotor with $B \sim C \sim 0.8$ cm^{-1} and in addition exhibits low frequency in-

† Electronic Supplementary Information (ESI) available: Detailed derivation of intensity ratios for the TTA analysis in the case of methanol, Extended details on experimental apparatus and supersonic expansion characterization, overview methanol spectra, and complete linelist of transitions included in the TTA and GSCD analysis. See text for details. See DOI: 10.1039/b000000x/

[a] *J. Heyrovský Institute of Physical Chemistry, Dolejškova 2155/3, 182 23 Prague 8, Czech Republic*
[b] *Institute of Chemical Technology Prague, Department of Physical Chemistry, Technická 5, 166 28 Prague 6, Czech Republic.*

ternal torsional vibration around the C-O bond. High resolution spectroscopic experiments on methanol were carried out mainly in the fundamental range and low-energy combination bands, see [16–19], but the overtone range is almost unexplored at high resolution due to its complexity and small absorption cross sections. The OH stretch overtones were studied at low resolution by Boyarkin, Perry, Rizzo, and Rueda using action spectroscopy, where OH-stretch excitation spectra were measured up to $8\nu_1$ [20–24]. Recently jet-cooled FTIR spectra of $2\nu_1$ overtone band with 2 cm^{-1} resolution were also reported[25]. Partial ro-vibrational analysis was carried out for several combination and overtone bands up to 11000 cm^{-1} including $2\nu_1$ band[24]. The only high resolution overtone spectra in the near IR has been the OH- and CH-stretch combination band centered around 6530 cm^{-1}, which has bee measured and analyzed in detail by Perry and coworkers[16].

Here we present first rotationally resolved spectra of the methanol $2\nu_1$ overtone band between 7180 – 7220 cm^{-1}. The measurements were carried out in a slit-jet supersonic expansion using cw-diode laser spectrometer. Spectra were measured at three different jet temperatures: 13, 23, and 56 K, respectively. Spectral resolution is limited by the residual Doppler broadening at the jet temperatures. Presented analysis is primarily focused on the applicability of two temperature technique for this molecule. In particular we demonstrate the technique for identifying the low-J transitions in the complex spectra and show how it helps with further confirmations by ground state combination differences (GSCDs). For the two temperature analysis (TTA) 13 and 56 K spectra were chosen. Spectrum at 23 K was used for further analysis by GSCDs. It is demonstrated, that the combination of these two approaches leads to reliable assignments of many spectral lines in the overtone spectra.

2 Ro-vibrational structure of methanol

Methanol is a near-prolate asymmetric top molecule with ground state rotational constants $\mathbf{A} = 4.259$ cm^{-1}, $\mathbf{B} = 0.824$ cm^{-1}, and $\mathbf{C} = 0.793$ cm^{-1}. Also, methanol is one of the simplest molecules with hindered internal rotation and/or torsional vibration. As a result the structure of rotational levels is complicated by interaction between the overall rotation and the torsional vibration ν_t.

Due to the finite torsion barrier, the ground torsional state is split into three levels that belong to two symmetry species – non-degenerate A component and doubly degenerate E component respectively. The A component rotational levels with $K > 0$ are further split in $A+$ and $A-$ levels due to asymmetry splitting and are labeled by $(J,K,A\pm)$ quantum numbers. The E state degeneracy is removed for $K \neq 0$ due to interaction between the torsional angular momentum and the over all rotation. The energy levels are labeled by signed value of K as $\pm K$

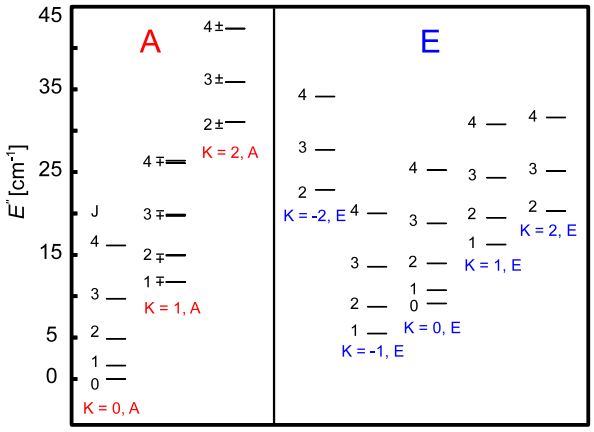

Fig. 1 Level diagram for the vibrational ground state of CH_3OH including quantum levels till $K'' = 2$ and $J'' = 4$ for A and E sub-band. The rotational energies were taken from reference[26].

respectively, according to relative orientation of the torsional and rotational angular momenta projection on the A-axis[26,27] and the E levels are therefore labeled as $(J,\pm K,E)$. As shown in figure 1 the three lowest rotational levels belong to the A symmetry. The lowest E symmetry state lies approximately 5.5 cm^{-1} above the lowest A level.[26]

The spectra consist of both perpendicular and parallel transitions given by selection rules:
A levels:
$+ \leftrightarrow +, - \leftrightarrow -, \Delta J = \pm 1, \Delta K = 0, \pm 1$ and
$+ \leftrightarrow -, \Delta J = 0, \Delta K = 0, \pm 1$
E levels:
$\Delta J = \pm 1, \Delta K = 0$ and
$\Delta J = 0, \pm 1, \Delta K = \pm 1$
From selection rules for the A levels follow that sub-band $K' = 0 \leftarrow K'' = 0$ does not have a Q-branch because all A levels with $K = 0$ have $+$ parity.

Two possible nuclear spin isomers exist in methanol due to the three equivalent hydrogen atoms on the methyl group. Total nuclear spin is $I_n = 3/2$ for the ortho nuclear spin isomer and $I_n = 1/2$ for para nuclear spin isomer. Due to the symmetry of total wavefunction the A and E rotation-torsional states are ortho and para nuclear spin states respectively[28,29]. The nuclear spin statistical weights for methanol are 4 and 2 for ortho and para isomers, respectively.

3 Two temperature analysis for methanol

Ratio of line intensities of given spectral transition measured at two different temperatures T_1 and T_2, respectively, is a quantity independent on line strength parameters and thus can be determined experimentally without any knowledge of the spectral line assignment. Under thermodynamic equilibrium

it is related to the lower state energy E'' of given transition via expression:

$$R_{th}(T_1,T_2) \equiv \frac{S(T_1)}{S(T_2)} = \frac{Q(T_2)}{Q(T_1)} e^{\frac{-E''}{k_B}\left(\frac{1}{T_1}-\frac{1}{T_2}\right)}. \quad (1)$$

where Q(T) are the rotatinal partition functions at the measurement temperatures:

$$Q(T) = \sum g_{T,o} \cdot g_{I,o} \cdot (2J+1) \cdot e^{\frac{-E''}{k_B T}}, \quad (2)$$

This relation has been used to calculate the lower state empirical energies E''_{exp}, and hence to deduce the lower states rotational quantum numbers, from the measured intensity ratios $R_{exp}(T_1,T_2)$ from spectra measured in absorption cells at various temperatures[3,5,7,8,30].

However, when experiments are performed in supersonic expansion this procedure must be modified, as thermodynamic equilibrium is generally not established under the rapid cooling. While rotational degrees of freedom are usually in equilibrium with the buffer gas temperature, equilibrium is not established between the nuclear spin isomers as the nuclear spin is in most cases conserved on the time scale of supersonic cooling. Under those conditions rotational partition functions differ for each nuclear spin isomer and therefore direct inversion of equation 1 to obtain E_{exp} from R_{exp} is not possible. Nevertheless for given choice of temperatures T_1 and T_2 every lower state rotational level still corresponds to specific value of intensity ratio $R(T_1,T_2)$ and relevant information on the lower rotational states can be extracted by matching the experimental intensity ratios R_{exp} to theoretically predicted values R_{th}.

Assuming that the nuclear spin is conserved during the supersonic cooling, partial partition functions $Q_{ortho}(T)$ and $Q_{para}(T)$ can be evaluated independently for each nuclear spin isomer:

$$Q_{ortho} = \sum_{ortho} g_{T,o} \cdot g_{I,o} \cdot (2J+1) \cdot e^{\frac{-E''}{k_B T}}, \quad (3)$$

$$Q_{para} = \sum_{para} g_{T,p} \cdot g_{I,p} \cdot (2J+1) \cdot e^{\frac{-E''}{k_B T}}. \quad (4)$$

and thus $R_{th}(T_1,T_2)$ can be calculated using equation 1 with appropriate partition functions for given rotational level. Values for 56 K and 13 K are presented in Table 1, using lower state energies E'' from[26]. Details of the intensity ratio evaluation procedure are given in ESI†.

Choice of the T_1 and T_2 temperatures determines the range of rotational energies where the two-temperature technique provides useful predictions. For $T_1 > T_2$ the $R(T_1,T_2)$ is exponentially decreasing with rising rotational energy E''. Highest ratio is obtained for the lowest energy level $E''=0$ and is equal to the partition function ratio $Q(T_1)/Q(T_2)$. The rate of the exponential decay with E'' is given by the factor $1/k_B(1/T_1 - 1/T_2)$.

Table 1 Theoretical value of intensity ratio $R_{th}(56,13)$ sorted according decreasing value of R_{th}. Table also summarises lower state energies E'' from[26]

lower rotational level	E''/cm^{-1}	$R_{th}(56,13)$
(0,0,A)	0.00000	11.42
(1,0,A)	1.61353	9.96
(1,-1,E)	5.48973	8.85
(2,0,A)	4.84048	7.57
(2,-1,E)	8.71660	6.73
(0,0,E)	9.12204	6.50
(1,0,E)	10.73572	5.67
(3,0,A)	9.68060	5.02
(3,-1,E)	13.55654	4.46
(2,0,E)	13.96277	4.31
(1,1,A+)	11.70493	4.22
(1,1,A-)	11.73276	4.21
(1,1,E)	16.24120	3.55
(2,1,A+)	14.90429	3.22
(2,1,A-)	14.98777	3.20
(4,0,A)	16.13354	2.90

Lower temperature T_2 generally determines the range of rotational levels included in the analysis. States with $E'' >> k_B T_2$ have negligible population and spectral lines originating from those levels have low intensity in the spectra. Clearly the choice of T_2 then depends on the nature of studied molecule - lower temperatures are needed for molecules with smaller rotational constants to eliminate high-J'' states. Practical choice of the lower temperature T_2 is often determined by experimental constrains such as the lowest attainable temperature in the supersonic expansion in the particular case of our experimental set-up.

Precision of lower state determination by TTA increases with incrasing T_1 for given value of T_2. For example, for $T_2 = T_1/2$ value of $R(T_1,T_2)$ decreases by a factor $1/e = 0.36$ when lower energy changes between $E''=0$ and $E'' = k_b \cdot T_1$ but this intensity ratio range increases to $1/e^2 = 0.13$ for $T_2 = T_1/3$, providing significantly improved lower energy resolution at given intensity uncertainty. Choice of the upper temperature is usually a compromise between the required resolution of the TTA and congestion of the spectrum at T_1.

This point is illustrated in Figure 2, where calculated values $R_{th}(T_1,T_2)$ are plotted as function of E'' for methanol rotational states with $E'' < 16$ cm^{-1} . The higher temperature is set to value $T_1 = 56$ K and predictions for two different values of T_2 are presented: 13 K and 23 K respectively. Those temperatures correspond to our experimental conditions, as discussed below. Different trends for A and E symmetry states (squares and triangles respectively) are due to the non-equilibrium distribution of the nuclear spin isomer

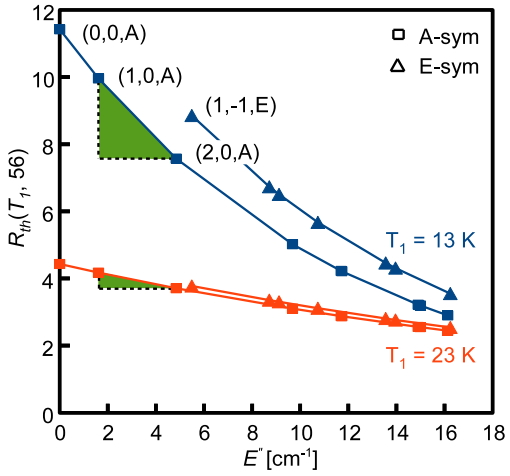

Fig. 2 Theoretical intensity ratio $R_{th}(56,T_2)$ dependence on the lower state rotational energy E'' for temperatures $T_1 = 13$ K and 23 K, respectively. Green triangles demonstrated a 2.1× better intensity ratio resolution at the lower temperature (13 K).

populations in the supersonic expansion. Wider spacing of the intensity ratios between individual rotational states is clearly demonstrated for $T_2 = 13$ K (blue lines and symbols online), compared to $T_2 = 23$ K (red lines and symbols online). Relative experimental error of $R(T_1,T_2)$ below approximately 10 % would be sufficient to distinguish uniquely the four lowest rotational states, $(0,0,A)$, $(1,0,A)$, $(2,0,A)$, and $(1,-1,E)$ at $T_2 = 13$ K, while the intensity measurement error below 5 % would be needed to resolve those states in the $T_2 = 23$ K case.

4 Experimental set up

Measurements were carried out with tunable diode laser direct-absorption spectrometer coupled with pulsed slit-jet supersonic nozzle source. The apparatus is briefly described in this section. For more details see[8,12,13]. Further details are also available in ESI†.

The high resolution extended cavity diode laser in Littmann configuration is used to record overtone infrared spectra in the range (7070 – 7300 cm^{-1}). The output power of the laser is 3 mW and the line width is typically 1 MHz. This is negligible compared to the residual Doppler line widths in the molecular beam (around 130 MHz). Part of the laser beam (around 10 %) is deflected to a custom built Michelson wavemeter and temperature stabilized Fabry - Pérot interferometer. Rest of the laser beam is equally split to reference and signal paths and are detected by custom autobalanced differential dual beam photodetector (design derived from Hobbs[31]) to reduce laser amplitude noise. The signal beam is double passed through the molecular beam along the slit axis.

The spectra are frequency calibrated using the Michelson wavemeter referenced to polarization stabilized He-Ne laser and stable Fabry - Pérot interferometer. Absolute laser frequency is determined using jet-cooled H_2O absorption line (7218.20009 cm^{-1})[32] which has been measured simultaneously with the methanol spectra. Reproducibility of laser frequency measurements is typically $3 \cdot 10^{-4}$ cm^{-1} while the absolute calibration is estimated to be better than $1 \cdot 10^{-3}$ cm^{-1} across the measured spectral range.

Molecular beam is produced by supersonic expansion through a slit nozzle (cross section of 0.1 x 40 mm^2) with solenoid actuated pulsed valve, which is a modified version of design by Lovejoy and Nesbitt[33]. The valve produces short ($\Delta t \leq 1$ ms), high intensity gas pulses typically at 3 Hz repetition rates. Such configuration permits high sensitivity direct absorption measurements with spectral resolution limited by residual Doppler line widths.

Expanding gas is a mixture of small amount of methanol in excess of a buffer gas (argon or helium). Methanol rotational temperature depends on expanding gas composition as well as on the total stagnation pressure and temperature. To maintain constant conditions over extended time periods new inlet system with two parallel input lines controlled by mass flow controllers has been constructed. One line is used for pure rare gas and second for rare gas saturated with methanol vapor at room temperature (partial pressure of CH_3OH at 298 K is $p_{298} = 126.05$ Torr). This system provides full control of methanol mixing ratio and the stagnation pressure P_0.

Wide range of expansion conditions have been tested (see ESI† for details). Argon expansion at 33.3kPa stagnation pressure with 0.3%, 1.6%, and 2.7% methanol volume fraction for the 13 K, 23 K, and 56 K temperatures, respectively, has been used for the presented data.

5 Results and discussion

5.1 High resolution spectra of OH-stretch overtone

Methanol absorption spectra were recorded in the region of 7180 – 7220 cm^{-1}, covering the most intense section of the $2\nu_1$ overtone band. Overview spectra measured at 13, 23, and 56 K respectively can be found in ESI†.

Short sections of the measured spectra near the band center are presented in Figure 3, demonstrating their simplification at reduced temperatures. Although the spectra at 56 K are less congested than at room temperature, number of observed transitions is still large with frequent overlaps. Only when the temperature is reduced down to 13 K, the overlaps gradually disappear, due to both line number and line width reduction. On the other hand peak absorbances are significantly reduced, because very low methanol concentration is required to reach such low temperatures.

All observed spectral lines were fitted by Gaussian line shape profile using Fityk program[34]. As the spectrum consists of many overlapped and weak lines, only selected strong and isolated lines were used to determine line widths (and hence the Doppler temperature) for given expansion conditions. The widths of weaker and/or blended lines were fixed to this common value to obtain more reliable line positions and intensities. We have observed 1071 lines lines with $S/N > 2$ on the line center at 56 K, 746 lines at 23 K, and 199 lines at 13 K.

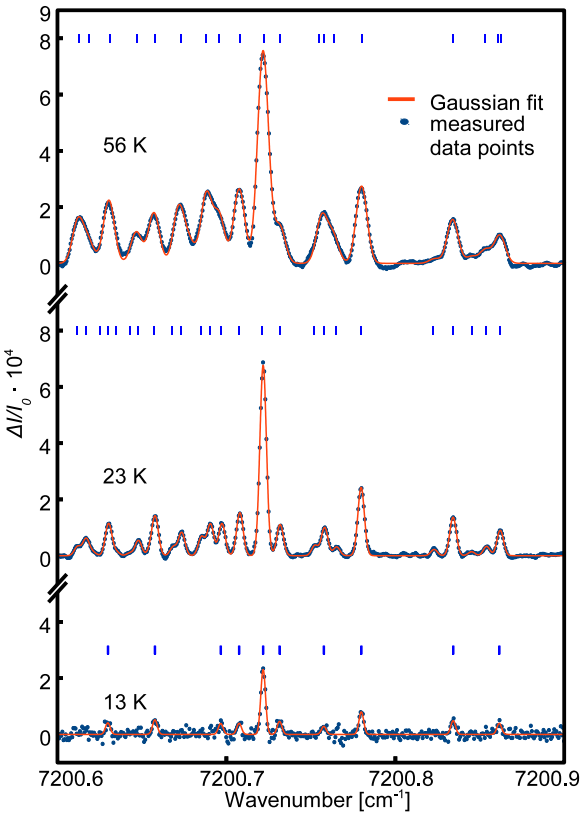

Fig. 3 Detail of spectra at 13, 23 and 56 K. Points represent experimental data, solid line is Gaussian multipeak fit with fixed FWHM to expansion temperature.

5.2 Two temperature analysis

In total 147 lines from 13 K spectral were linked with corresponding transitions at 56 K based on the frequency coincidence (difference less than 0.002 cm^{-1}). These transitions were further divided into two groups according their intensities in the 13 K spectrum. The first group consists of 37 most intense lines in the with integrated absorbances $\Sigma_{13K} > 4.04 \cdot 10^{-7}$ cm^{-1}. Those spectral lines most likely originate from the lowest rotational states of the principal vibrational bands in the covered spectral region.

Integrated absorbances $\Sigma(T)$ are related to experimental intensity ratios $R_{exp}(T_1,T_2)$ via equation:

$$\frac{\Sigma(T_1)}{\Sigma(T_2)} = f(T_1,T_2)\cdot R_{exp}(T_1,T_2), \quad (5)$$

where the scaling factor

$$f(T_1,T_2) \equiv \frac{N_u(T_1)}{N_u(T_2)}. \quad (6)$$

$N_u(T)$ is methanol integrated column density along the absorption path. In general the scaling factor depends on methanol concentration profile and has the same value for all spectral lines under given experimental conditions (for more detail see ESI†). For example, in cell experiments where the number density N_0 and absorption path length l are temperature independent $f(T_1,T_2) = 1$. In supersonic jet experiments however the expansion conditions are varied to control the temperature and therefore the molecular number density and to some extend even the absorption path length are different at T_1 and T_2 respectively and the correction factor $f(T_1,T_2)$ must be determined for given experimental conditions.

This is done in two steps - first, approximate value is obtained as the ratio of methanol concentrations in the gas mixtures used for the 13 K and 56 K spectra. Since the flow rate of methanol changes by a factor of 10x between the 13 K and 56 K expansion conditions $f(56K,13K) = 10$. This value is used for preliminary assignments by the TTA for several transitions with the highest intensity in the 13 K spectrum. This initial assignment is further simplified by the fact, that regardless of the correction factor, highest intensity ratios always correspond to the lowest ground state rotational energies, see Figure 2 and Table 1. Next, those preliminary TTA assignments are confirmed by the ground state combination differences as discussed in details below and one of those reliably assigned lines is used to re-evaluate the correction factor to match the theoretical value of intensity ratio.

Specifically, we have chosen the strongest spectral line observed at 7205.3378 cm^{-1}. Based on the estimated value of the normalization factor $f = 10$ this transition has $R_{exp} = 10.4$, consistent with the lower state assignment to $(0,0,A)$ rotational level. This preliminary assignment has been verified using ground state combination differences and then this transition has been used for correcting the normalization factor to value $f = 11$ to bring the experimental value of intensity ratio R_{exp} to agreement with predicted value $R_{th} = 11.42$ for this particular ground state level. This improved value of normalization factor has subsequently been applied for evaluating R_{exp} for all other spectral lines.

For given choice of T_1 and T_2, reliability of the TTA procedure depends on experimental error of intensity measurements. Those errors determine uncertainty of R_{exp} which in

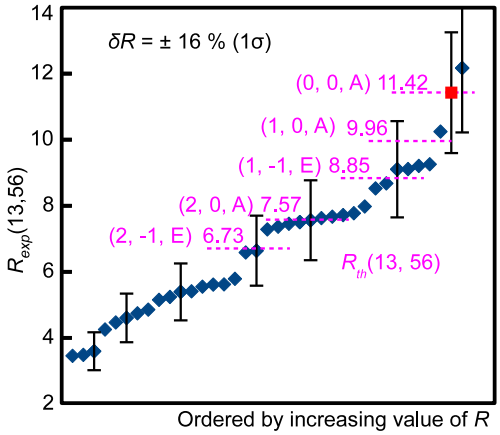

Fig. 4 Experimental intensity ratios $R(13,56)$ for lines in the first group, eg. with $\Sigma_{13K} > 4.04 \cdot 10^{-7}$ cm^{-1}. Dashed lines and associated values represent the theoretical intensity ratios R_{th} with corresponding lower state assignments (all pink in on-line version). Transition used for calibration of correction factor f is highlighted in red square.

turn define a range of possible values that are consistent with given experimental intensity ratio. All the rotational states with predicted intensity ratios R_{th} within those experimental error margins must be considered as lower states candidates. Clearly TTA assignment is more specific for small intensity errors. In the presented experiments intensity ratio error was determined to be $\delta R_{exp} = 16\%(1\sigma)$ based on repeated measurements of line intensities for set of 51 selected transitions.

Figure 4 demonstrates matching between experimental and theoretical intensity ratios. Here the R_{exp} values of the 37 strongest transitions are plotted in order of increasing value. In this representation of data, transitions with similar R_{exp} values are grouped together. Vertical error bars indicate the estimated error δR_{exp}, while dashed horizontal lines (pink online) indicate the theoretical intensity ratios R_{th} for the five lowest methanol rotational levels. In absence of any experimental error, this plot should exhibit a step-vice structure with plateaus corresponding to theoretical ratio values of transitions that originate from individual rotational states. With experimental scatter, those plateaus became sloping and eventually individual steps would blend for large experimental errors. While some of those steps are discernible in the presented data and match well the predicted ratios, they are less pronounced compared to similar plots for CH_4 and NH_3 [8,9,12].

This observation is consistent with the much smaller energy spacing between individual rotational levels of CH_3OH compared to those lighter molecules. Indeed the presented error bars, which are probably somewhat conservative, are comparable in amplitude with the expected steps as defined by theoretical intensity ratios. Therefore the TTA in the case of CH_3OH provides (with current intensity error bars) a range of possible lower rotational states for given transition (typically 2 – 4). Those possible empirical assignments for all transitions from the high-intensity data subset are listed in Table 2.

5.3 Analysis by GSCDs

Based on the TTA, 21 lines with $R_{exp} > 6$ are indicated as candidates for transitions from one of the four lowest rotational states (listed in Table 2) and were subject to further analysis using ground state combination differences (GSCDs) to confirm their assignments. This analysis was done using the spectrum measured at 23 K, that consists of more transitions than the spectrum measured at 13 K but has significantly less overlaps compared to the spectrum measured at 56 K.

Selection rules for CH_3OH allow 2 transitions from the $(0,0,A)$ level, specifically parallel ${}^qR(0)$ and perpendicular ${}^rR(0)$ transition. ${}^qR(0)$ shares the upper state with 3 other transitions: From $(1,1,A-)$, $(2,0,A)$, and $(2,1,A+)$ lower states. The ${}^rR(0)$ has exactly the same 3 combination differences plus one additional originating from state $(2,2,A+)$. This means that while observation of the first three combination differences unambiguously determines the lower state as $(0,0,A)$, it is the existence of this fourth combination difference that distinguishes between the transitions. Schematic diagrams with combination differences for this level can be found in ESI†.

In analogy with the $(0,0,A)$ case, it can be shown, that every transition from $(1,0,A)$ level must have combination difference with $(1,1,A+)$ level and that each transition from $(2,0,A)$ level must have combination difference with $(2,1,A+)$ level. However there is no common combination difference in the case of $(1,-1,E)$ level.

Analysis of the pre-selected transitions using the GSCD was done as follows: At first we assumed that all of the 21 highlighted transitions can originate from any of the four lowest rotational states. Based on knowledge of the ground state energies we calculated appropriate GSCDs for each rotational level and thus predicted line positions by GSCDs, provided the given line starts from the expected rotational level. When a line is observed at the predicted position with accuracy better than $\delta\nu < 0.001$ cm^{-1}, the GSCDs is considered to be correct. Lines were assigned to specific transitions only if all necessary combination differences were found.

The procedure leads to assignment of 15 lines from the group of 21 transitions pre-selected by TTA listed in Table 2. Remaining 6 transitions probably originate from slightly higher ground rotational states such as $(1,-1,E)$, $(1,-1,E)$, or $(1,-1,E)$ respectively. This is consistent with the TTA yet has not been explicitly tested by GSCD at this point. Moreover, number of additional lines were confirmed (listed in the ESI†), for 7 of them the TTA information is also available (marked by * in ESI†).

Table 2 Transitions from four lowest rotational states $(0,0,A)$, $(1,0,A)$, $(2,0,A)$, and $(1,-1,E)$, based on TTA analysis.

position/cm^{-1}	[a] Σ_{13K}/cm^{-1}	$R_{exp}(13,56)$	[b] TTA LS (1σ)	[c] GSCD LS	Transition	[d] TTA Error/%
7206.9078	1.189E-06	12.17	(0,0,A), (1,0,A)	(1,0,A)	$^{r}R1$	22.19
7205.3378	1.220E-06	11.42	(0,0,A), (1,0,A)	(0,0,A)	$^{r}R0$	0.00
7196.3742	4.064E-07	10.25	(0,0,A), (1,0,A), (1,-1,E)	(1,-1,E)		15.71
7198.1151	6.236E-07	9.26	(0,0,A), (1,0,A), (1,-1,E), (2,0,A)	(0,0,A)	$^{q}R0$	-18.96
7208.4607	1.107E-06	9.21	(1,0,A), (1,-1,E), (2,0,A)	(2,0,A)	$^{r}R2$	21.63
7197.8219	7.028E-07	9.11	(1,0,A), (1,-1,E), (2,0,A)	(0,0,A)	$^{q}R0$	-20.23
7195.9195	1.407E-06	9.11	(1,0,A), (1,-1,E), (2,0,A)			
7194.9242	4.846E-07	8.68	(1,0,A), (1,-1,E), (2,0,A)	(1,0,A)	$^{q}P1$	-12.86
7194.6216	7.246E-07	8.53	(1,0,A), (1,-1,E), (2,0,A)	(1,0,A)	$^{q}P1$	-14.38
7209.9897	5.074E-07	7.98	(1,-1,E), (2,0,A), (2,-1,E)			
7193.2745	7.285E-07	7.78	(1,-1,E), (2,0,A), (2,-1,E), (0,0,E)	(2,0,A)	$^{q}P2$	2.71
7200.7218	7.812E-07	7.72	(1,-1,E), (2,0,A), (2,-1,E), (0,0,E)			
7199.6677	1.279E-06	7.67	(1,-1,E), (2,0,A), (2,-1,E), (0,0,E)	(1,0,A)	$^{q}R1$	-22.99
7201.2638	5.451E-07	7.63	(1,-1,E), (2,0,A), (2,-1,E), (0,0,E)	(2,0,A)	$^{q}R2$	0.76
7202.3472	4.749E-07	7.56	(1,-1,E), (2,0,A), (2,-1,E), (0,0,E)			
7201.2051	1.298E-06	7.51	(1,-1,E), (2,0,A), (2,-1,E), (0,0,E)	(2,0,A)	$^{q}R2$	-0.83
7192.6928	9.840E-07	7.46	(1,-1,E), (2,0,A), (2,-1,E), (0,0,E)			
7202.3270	6.577E-07	7.37	(1,-1,E), (2,0,A), (2,-1,E), (0,0,E)	(1,-1,E)	$^{r}P1-$	-16.80
7192.9815	8.154E-07	7.29	(1,-1,E), (2,0,A), (2,-1,E), (0,0,E)	(2,0,A)	$^{q}P2$	-3.76
7197.9782	4.851E-07	6.64	(2,0,A), (2,-1,E), (0,0,E), (1,0,E)	(1,-1,E)	$^{r}Q2-$	-25.02
7195.9416	6.294E-07	6.59	(2,0,A), (2,-1,E), (0,0,E), (1,0,E)			

[a] Integrated line intensities in the 13 K spectrum, [b] lower state assignments consistent with TTA, [c] lower state asssignment determined by GSCD, [d]Relative deviation of experimental intensity ratios from theoretical values for GSCD confirmed transitions as defined in Equation 7

It is useful to utilize those transitions whose assignemnts have been confirmed by GSCD to evaluate reliability of the TTA procedure by comparing their experimental intensity ratios to theoretical values. This comparison is presented in the form of correlation plot in Figure 5. Diagonal solid line (blue online) represents the perfect agreement between R_{exp} and R_{th}. Shaded area (green online) encompasses the range of experimental values that fall within error bars $2 \cdot \delta R_{exp}$ as determined from uncertainty of repeated intensity measurements. Statistically, 95 % of the transitions are expected to lie within this shaded area. Indeed, majority of the tested spectral lines fall within this range, indicating that the TTA gives predicions consistent with the actual lower state assignments. Two transitions in the figure do not lie within this interval (highlighted in red), indicating disagreement. However, these transitions start from higher rotational states and therefore have low intensity in the 13 K spectrum (less than 10 % integrated intensity of the strongest line) and thus their line strength uncertainty might be higher than estimated by the simple statistical error analysis.

Agreement between TTA and GSCDs analysis is also quantitatively described through the error parameter listed in the last column in Tab. 2 defined as:

$$\mathrm{Er}[\%] \stackrel{\mathrm{def}}{=} \frac{R_{exp} - R_{th}}{R_{th}} \times 100\%, \qquad (7)$$

It is interesting to note, that even within this very preliminary analysis three transitions from $(0,0,A)$ level were found,

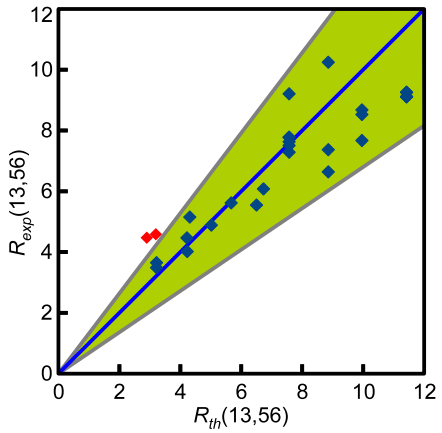

Fig. 5 Correlation between R_{th} derived from GSCDs and R_{exp} derived from TTA, highlighting the agreement between TTA and GSCDs analysis respecitvely. In the case of perfect agreement all point would lie on the diagonal. The shaded area (green online) represents experimental error $2 \cdot \delta R_{exp}$. Only two transitions highlighted in red exhibit statistically significant disagreement (lie outside the green area).

namely 7197.8219, 7198.1151, and 7205.3378 cm^{-1}. Since each vibrational band has only two ro-vibrational transitions starting from $(0,0,A)$ state, we must conclude that another vibrational band expect the $2\nu_1$ is presented in this spectral region. Due to the high complexity of overtone spectra and many perturbations, we have not found so far the fourth transition of the $(0,0,A)$ state.

6 Conclusion

We have presented first high resolution methanol spectrum in the OH-stretch overtone $2\nu_1$ region (7180 – 7220 cm^{-1}) by diode laser near infrared spectrometer in supersonic slit jet expansion. Three spectra were measured at 13, 23, and 56 K respectively. Spectra measured at 13 and 56 K were used to estimate lower state rotational states by the two temperature analysis for 147 spectral lines. While the two temperature analysis does not provide unique assignments in this case, it still yields a restricted set of possible lower rotational states. This information has further been coupled with the method of ground state combination differences to provide reliable spectral assignments for a sub-set of spectral lines from few lowest rotational states. This combined method is shown to be efficient tool in determination of ro-vibrational transitions in dense overtone regions and will be used in future analysis of the complicated methanol spectra.

Acknowledgement
We are grateful to Li-Hong Xu for fruitful discussions regarding the methanol ground state energies and to Michal Farnik for help and support. This work was supported by the Czech Science Foundation under Grant 13-11635S.

References

1 J. S. Margolis, *Appl. Opt.*, 1990, **29**, 2295.
2 L. Brown and J. Margolis, *Journal Of Quantitative Spectroscopy & Radiative Transfer*, 1996, **56**, 283–294.
3 A. Campargue, O. Leshchishina, D. Mondelain, S. Kassi and A. Coustenis, *Journal of Quantitative Spectroscopy and Radiative Transfer*, 2013, **118**, 49–59.
4 B. Gao, S. Kassi and A. Campargue, *Journal of Molecular Spectroscopy*, 2009, **253**, 55–63.
5 K. Sung, L. R. Brown, X. Huang, D. W. Schwenke, T. J. Lee, S. L. Coy and K. K. Lehmann, *Journal of Quantitative Spectroscopy and Radiative Transfer*, 2012, **113**, 1066–1083.
6 L. Wang, S. Kassi, A. Liu, S. Hu and A. Campargue, *Journal of Quantitative Spectroscopy and Radiative Transfer*, 2011, **112**, 937–951.
7 A. Campargue, L. Wang, D. Mondelain, S. Kassi, B. Bézard, E. Lellouch, A. Coustenis, C. de Bergh, M. Hirtzig and P. Drossart, *Icarus*, 2012, **219**, 110–128.
8 A. Campargue, L. Wang, S. Kassi, M. Mašát and O. Votava, *Journal of Quantitative Spectroscopy and Radiative Transfer*, 2010, **111**, 1141–1151.
9 P. Cacciani, P. Cermak, J. Cosléou, M. Khelkhal, P. Jeseck and X. Michaut, *Journal of Quantitative Spectroscopy and Radiative Transfer*, 2012, **113**, 1084–1091.
10 L. Brown, K. Sung, D. Benner, V. Devi, V. Boudon, T. Gabard, C. Wenger, A. Campargue, O. Leshchishina, S. Kassi and et al., *Journal of Quantitative Spectroscopy and Radiative Transfer*, 2013, **130**, 201–219.
11 P. Cermak, J. Hovorka, P. Veis, P. Cacciani, J. Cosleou, J. El Romh and M. Khelkhal, *Journal of Quantitative Spectroscopy & Radiative Transfer*, 2014, **137**, 13–22.
12 M. Mašát, P. Pracna, D. Mondelain, S. Kassi, A. Campargue and O. Votava, *Journal of Molecular Spectroscopy*, 2013, **291**, 9–15.
13 O. Votava, M. Mašát, P. Pracna, S. Kassi and A. Campargue, *Physical Chemistry Chemical Physics*, 2010, **12**, 3145.
14 O. Votava, M. Mašát, P. Pracna, D. Mondelain, S. Kassi, A. Liu, S. Hu and A. Campargue, *Journal of Quantitative Spectroscopy and Radiative Transfer*, 2014, **149**, 64–71.
15 V. Svoboda, J. Rakovský and O. Votava, *Using Jet-Two-Temperature-Technique to reveal complicated overtone spectra of ammonia in 1.5 μm region*, 2014, manuscript in preparation.
16 S. Xu, J. J. Kay and D. S. Perry, *Journal of Molecular Spectroscopy*, 2004, **225**, 162–173.
17 R. Lee, R. H. Hunt, E. K. Plyler and D. M. Dennison, *Journal of Molecular Spectroscopy*, 1975, **57**, 138–154.
18 P. Carrick, R. Curl, M. Dawes, E. Koester, K. K. Murray, M. Petri and M. L. Richnow, *Journal of Molecular Structure*, 1990, **223**, 171–184.
19 I. Kleiner, G. Fraser, J. Hougen and A. Pine, *Journal of Molecular Spectroscopy*, 1991, **147**, 155–172.
20 O. Boyarkin, L. Lubich, R. Settle, D. Perry and T. Rizzo, *Journal of Chemical Physics*, 1997, **107**, 8409–8422.
21 O. V. Boyarkin, T. R. Rizzo and D. S. Perry, *The Journal of Chemical Physics*, 1999, **110**, 11359.
22 O. V. Boyarkin, T. R. Rizzo and D. S. Perry, *The Journal of Chemical Physics*, 1999, **110**, 11346.
23 D. Rueda, O. V. Boyarkin, T. R. Rizzo, A. Chirokolava and D. S. Perry, *The Journal of Chemical Physics*, 2005, **122**, 044314.
24 D. Rueda, O. V. Boyarkin, T. R. Rizzo, I. Mukhopadhyay and D. S. Perry, *The Journal of Chemical Physics*, 2002, **116**, 91.
25 F. Kollipost, K. Papendorf, Y.-F. Lee, Y.-P. Lee and M. A. Suhm, *Physical Chemistry Chemical Physics*, 2014, **16**, 15948–15956.
26 L. Xu and J. Hougen, *Journal of Molecular Spectroscopy*, 1995, **169**, 396–409.
27 R. M. Lees, *The Astrophysical Journal*, 1973, **184**, 763–771.
28 G. Herzberg, *Molecular Spectra and Molecular Structure II. Infrared and Raman Spectra of Polyatomic Molecules*, D. Van Nostrand Company, Inc., 1945.
29 M. Hepp, I. Pak, K. Yamada, E. Herbst and G. Winnewisser, *Journal of Molecular Spectroscopy*, 1994, **166**, 66–78.
30 A. Campargue, O. Leshchishina, L. Wang, D. Mondelain, S. Kassi and A. Nikitin, *Journal of Quantitative Spectroscopy and Radiative Transfer*, 2012, **113**, 1855–873.
31 P. C. D. Hobbs, *Appl. Opt.*, 1997, **36**, 903.
32 L. Rothman, D. Jacquemart, A. Barbe, D. Chris Benner, M. Birk, L. Brown, M. Carleer, C. Chackerian, K. Chance, L. Coudert and et al., *Journal of Quantitative Spectroscopy and Radiative Transfer*, 2005, **96**, 139–204.
33 C. M. Lovejoy and D. J. Nesbitt, *Review of Scientific Instruments*, 1987, **58**, 807.
34 M. Wojdyr, *J Appl Cryst*, 2010, **43**, 1126–1128.